ACS Photonics
Letter
pubs.acs.org/journal/apchd5

# Sequential Deposition of $CH_3NH_3PbI_3$ on Planar NiO Film for Efficient Planar Perovskite Solar Cells

Long Hu,[†,‡] Jun Peng,[§] Weiwei Wang,[§] Zhe Xia,[†,‡] Jianyu Yuan,[§] Jialing Lu,[§] Xiaodong Huang,[§] Wanli Ma,*[,§] Huaibing Song,[†,‡] Wei Chen,[†] Yi-Bing Cheng,[†,∥] and Jiang Tang*[,†,‡]

[†]Wuhan National Laboratory for Optoelectronics (WNLO) and [‡]School of Optical and Electronic Information, Huazhong University of Science and Technology, Wuhan, Hubei 430074, China

[§]Institute of Functional Nano & Soft Materials (FUNSOM), Soochow University, Suzhou, Jiangsu 215123, China

[∥]Department of Materials Engineering, Monash University, Wellinton Road, Clayton, Victoria 3800, Australia

**ABSTRACT:** The new emerging organometal trihalide perovskite holds great potential for high-efficiency, low-cost solar cells because of its high solar to electricity conversation efficiency (>16%) achieved within 4 years of research and its low-temperature solution processing. In this Letter we introduce NiO as the hole-collecting and -conducting layer in perovskite solar cells. Through a modified sequential deposition strategy, we successfully fabricated high-quality $CH_3NH_3PbI_3$ onto a planar NiO layer and built a planar inverted ITO/NiO/$CH_3NH_3PbI_3$/PCBM/Al photovoltaic device. A device efficiency of 7.6% was achieved with an impressively high open-circuit voltage ($V_{oc}$) of 1.05 V. Our study demonstrates the potential application of a deep work function NiO layer for perovskite solar cells.

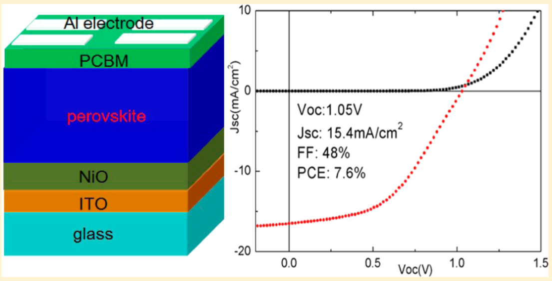

**KEYWORDS:** *perovskite, solar cell, NiO, sequential deposition*

High-efficiency, low-cost solar cells are the everlasting pursuit of photovoltaic research. Very recently, organometal halide perovskite has attracted tremendous research attention because of its potential to realize this goal. First introduced in 2009 by Miyasaka's group as the sensitizer for dye-sensitized solar cells (DSSCs) using liquid electrolyte,[1] organometal halide perovskites gradually evolved to solid-state DSSCs by incorporating triarylamine derivative 2,2′,7,7′-tetrakis(*N,N*-di-*p*-methoxyphenylamine)-9,9′-spirobifluorene (spiro-MeOTAD)[2] or other materials[3,4] as the hole-transporting and -collecting layer and finally developed into the current form of a planar p−i−n heterojunction device configuration.[5,6] State-of-the-art perovskite solar cells include sequentially deposited $CH_3NH_3PbI_3$ to sensitize a mesoporous $TiO_2$ electrode and achieved 14.1% certified device efficiency[7] and also include a thermally evaporated $CH_3NH_3PbI_{3-x}Cl_x$ absorber to build 15.4% planar heterojunction solar cells.[5] This soaring conversion efficiency, coupled with their simple device fabrication process, enables the perovskite solar cell to be a very promising candidate for high-efficiency, low-cost photovoltaics.[8,9]

Similar to other absorber materials in solar cells, organometal trihalide perovskite is capable of efficient and balanced electron and hole transport. Diffusion lengths of more than 100 nm for $CH_3NH_3PbI_3$[10] and more than 1000 nm for $CH_3NH_3PbI_{3-x}Cl_x$[11] were reported from a femtosecond transient optical spectroscopy study and transient absorption and photoluminescence-quenching measurements, respectively. As a result, planar heterojunction device configurations are gradually attracting more attention because removal of the mesoscopic layer simplifies device preparation and reduces materials cost. Many planar device architectures, such as $TiO_2$/perovskite/spiro-MeOTAD,[5] PEDOT:PSS/perovskite/$C_{60}$,[12,13] and ZnO/perovskite/spiro-MeOTAD,[6] were reported, with the best efficiency achieving 15.7%,[13] competing favorably with perovskite solar cells employing mesoscopic layers. One additional benefit, not yet fully demonstrated in perovskite solar cells but widely accepted in traditional thin-film photovoltaic fields, is the reduced heterojunction interface area in planar devices. For a heterojunction device, the reverse saturation current is proportional to the junction area; minimizing the interface area will minimize possible leakage channels, reduce reverse saturation current density, and improve device efficiency.

In this Letter, we present the fabrication of planar $CH_3NH_3PbI_3$ heterojunction solar cells. The device architecture is ITO/NiO/$CH_3NH_3PbI_3$/PCBM/Al, where ITO stands for indium-doped tin oxide and PCBM stands for [6,6]-phenyl-$C_{61}$-butyric acid methyl ester. NiO is a cubic p-type material with a large band gap widely applied in photovoltaic devices as a hole-conducting and -collecting layer;[14,15] however, the successful exploration of NiO in perovskite solar cells has not yet been reported. We chose NiO over $TiO_2$ because light-induced desorption of surface-adsorbed oxygen on $TiO_2$

**Received:** January 9, 2014
**Published:** June 18, 2014

severely degraded perovskite solar cell performance when they were subjected to long-term sunlight exposure.[16] The advantages of NiO over previously explored PEDOT:PSS are its inertness without corrosion to ITO substrates and its deeper work function, which would promise higher open-circuit voltages ($V_{oc}$). In addition, this new inverse device architecture (from the viewpoint of traditional DSSCs), with holes flowing to the ITO substrate instead of the traditional device involving $TiO_2$, where electrons flow to the ITO substrate, will expand the choice of selection for the integration of perovskite solar cells with silicon or copper indium gallium selenide (CIGS) solar cells to build tandem devices and target >40% device efficiency.[8] Using an improved sequential deposition strategy, we successfully deposited high-quality $CH_3NH_3PbI_3$ film onto NiO film and obtained a solar conversion efficiency of 7.6% from this inverse planar heterojunction device. Moreover, due to the deep work function of the NiO layer ($E_F = -5.26$ eV), a high open-circuit voltage ($V_{oc}$) of 1.05 eV was obtained, showcasing the promise of using NiO as a hole-collecting layer in perovskite solar cells.

## ■ EXPERIMENTAL SECTION

**NiO Film and $CH_3NH_3I$ Fabrication.** We first prepared NiO precursor solutions by adding nickel acetate tetrahydrate (Sinopharm Chemical reagent Co. Ltd., >98%) and monoethanolamine (Alfa) in methoxyethanol (Tokyo Chemical Industry Co. Ltd., >99%) and stirring overnight. Precursor solutions with nickel acetate weight percentages of 1%, 2%, 5%, 10%, and 15% were prepared to fabricate NiO film of different thicknesses. Prepatterned ITO glass substrates were cleaned by sequential ultrasonic treatment in acetone, detergent, acetone, isopropyl alcohol, and acetone and then were treated with UV-ozone (Seabiscuit-trade) for 30 min. Nickel acetate solution was spin-coated at 4000 rpm for 30 s on the ITO substrates, then annealed on a hot plate at 150 °C for 5 min, 250 °C for 10 min, and 350 °C for 60 min, all in air. When naturally cooled to room temperature, the NiO film was subjected to UVO treatment in a UV-ozone cleaner for 10 min. Methylamine (33 wt % in ethanol; Alfa) and hydroiodic acid (57 wt % in water; Alfa) were stirred at 0 °C for 2 h. After the reaction, the solvent in solution was evaporated with a rotary evaporator. A white powder, methylammonium iodide, was obtained and subsequently dissolved in ethanol and precipitated with diethyl ether. This process was repeated three times, and finally the products were dried at 60 °C in a vacuum for 24 h. A 300 mg/mL $PbI_2$ solution was prepared by dissolved $PbI_2$ in anhydrous *N,N*-dimethylformamide (DMF; Alfa) at 60 °C and stirred for 12 h inside a nitrogen-filled glovebox with oxygen and moisture levels of <0.5 ppm.

**Device Fabrication.** All the processes were carried out inside the nitrogen-filled glovebox. $PbI_2$ film was prepared by spin-coating a $PbI_2$ DMF solution onto a NiO surface at 3000 rpm for 30 s, baked on a 70 °C hot plate for 1 h, then dipped into a 10 mg/mL $CH_3NH_3I$ anhydrous isopropyl alcohol solution (this solution was preheated to 70 °C), kept at 70 °C for 45 s, and finally flushed with anhydrous isopropyl alcohol for 10 s. This film was further baked on a 70 °C hot plate for 20 min to finish the formation of $CH_3NH_3PbI_3$. After the perovskite film cooled to room temperature, a 20 mg/mL PCBM solution in chloroform was spin-coated on top at 1500 rpm for 30 s. Aluminum electrodes (about 100 nm) were thermally evaporated (1 Å/s) onto the PCBM layers under the pressure of $1 \times 10^{-6}$ mbar through a shadow mask. The active device area was 7.25 $mm^2$.

**Measurement and Characterization.** The current density–voltage characteristics of the devices were measured using a Keithley 2400 ($I-V$) digital source meter under a simulated AM 1.5G solar irradiation at 100 $mW/cm^2$ (Newport, AAA solar simulator, 94023A-U) inside the glovebox. Ultraviolet photoemission spectroscopy (UPS) measurement was carried out in a Kratos AXIS Ultra-DLD ultra-high-vacuum photoemission spectroscopy system with an Al K$\alpha$ radiation source.

Tapping mode atomic force microscopy (AFM) was performed using a Veeco multimode V instrument. Scanning electron microscopy (SEM) images were obtained using a FEI Nova NanoSEM 450. X-ray diffraction (XRD) results were acquired using a Phillips X'Pert PRO. Photoluminescence spectra were obtained by using an automated spectrofluorometer (FluoMax, Horiba Jobin-Yvon). NiO layer thickness was obtained by deposition of a NiO layer onto a Si wafer and measured by ellipsometry (J. A. Woollam Corporation, Alpha-SE).

## ■ RESULTS AND DISCUSSION

Various approaches were reported to build the NiO film including pulse laser deposition,[14] sputtering,[17] and solution processing;[18,19] we chose solution processing here because of its simple and low-cost fabrication. The planar NiO layer was first fabricated on the ITO substrate by spin-coating a nickel acetate ($Ni(CH_3COO)_2$) methoxyethanol solution and subsequently annealed at elevated temperature in the ambient atmosphere. Direct deposition of organometal trihalide perovskite onto planar NiO is difficult because of the poor adhesion between perovskite and the NiO layer. Snaith's group explored the planar NiO/$CH_3NH_3PbI_{3-x}Cl_x$/PCBM solar cells and obtained <0.1% device efficiency due to the very poor $CH_3NH_3PbI_{3-x}Cl_x$ coverage on the NiO surface.[13] We thus turned to the sequential deposition strategy to circumvent this challenge, as schematically shown in Figure 1. A $PbI_2$ layer of 180 nm thickness was first spin-coated from a 300 mg/mL DMF solution and baked at 70 °C inside a $N_2$-filled glovebox to evaporate the DMF. Afterward, this warm film was directly immersed into a 10 mg/mL $CH_3NH_3I$ isopropyl alcohol solution (preheated to 70 °C), kept at 70 °C for 45 s, rinsed with anhydrous isopropanyl alcohol for 10 s, and finally baked on a 70 °C hot plate for 20 min to complete the $CH_3NH_3PbI_3$ layer. Under such circumstances, $PbI_2$ worked as a seed layer, and the poor adhesion of $CH_3NH_3PbI_3$ on the planar NiO layer was resolved, yielding a shiny black perovskite film.

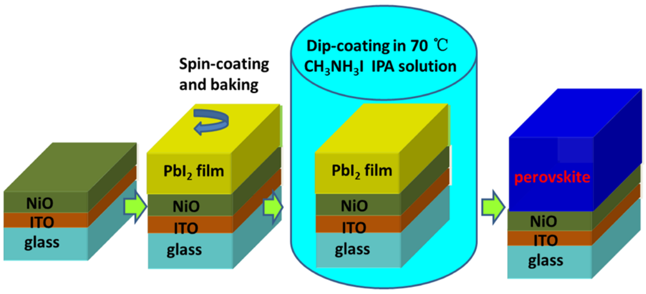

**Figure 1.** Schematic illustration of the sequential deposition of a $CH_3NH_3PbI_3$ layer onto a planar NiO film.

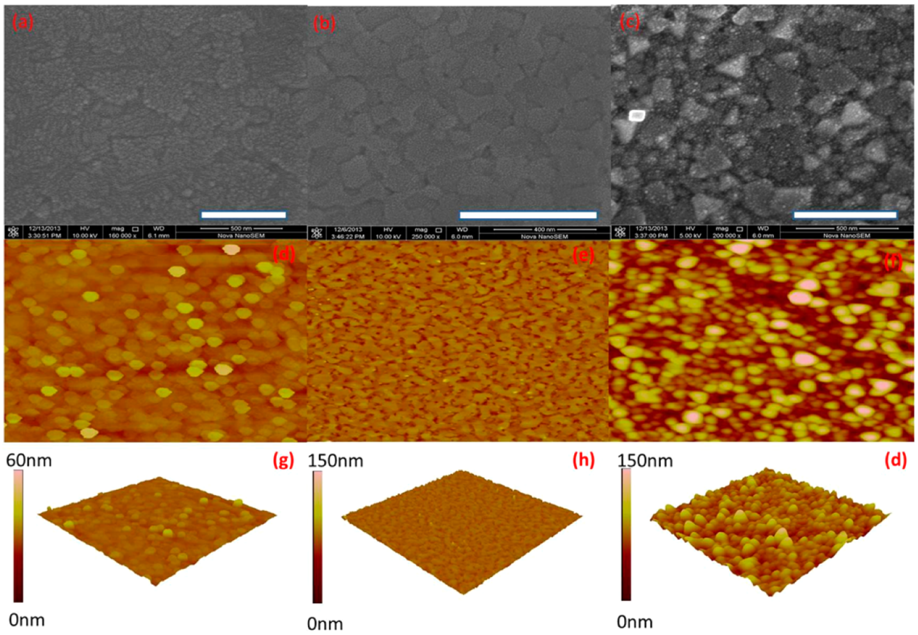

**Figure 2.** Top-view SEM and AFM images of (a, d, g) the NiO film; (b, e, h) a spin-coated $PbI_2$ layer on the NiO film; and (c, f, i) a sequentially deposited $CH_3NH_3PbI_3$ film on a planar NiO film. Scale bars for all SEM images are 500 nm, and the AFM image sizes are 5 × 5 μm.

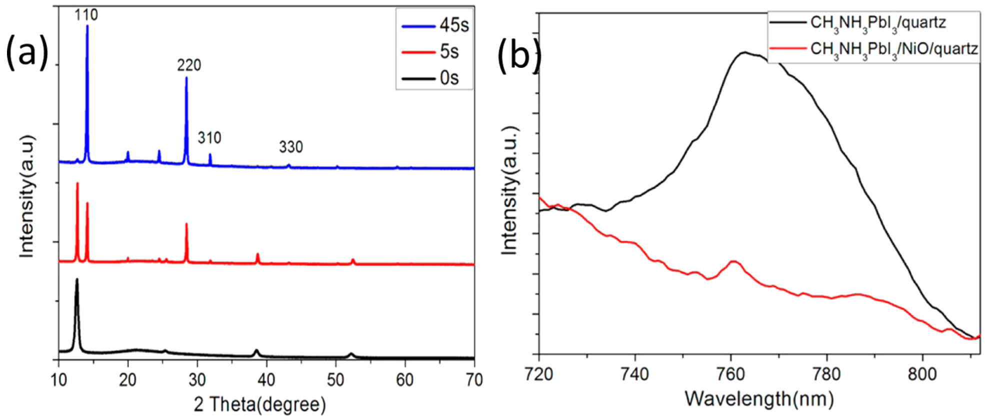

**Figure 3.** (a) XRD patterns for the transformation of $PbI_2$ into $CH_3NH_3PbI_3$. Insets are the reaction durations at 70 °C. The black curve is the XRD pattern of $PbI_2$. (b) Photoluminescence spectra (excited by 600 nm laser) of $CH_3NH_3PbI_3$ film deposited on top of NiO film or quartz substrate.

We first applied SEM and AFM to characterize film morphology and surface roughness of as-deposited NiO, $PbI_2$, and $CH_3NH_3PbI_3$ layers. The results are given in Figure 2. NiO was produced as the decomposition product of $Ni(CH_3COO)_2$ in air at elevated temperature. Top-view SEM and AFM studies revealed that our NiO film was composed of nickel oxide nanoparticles and the whole film was smooth and crack-free. AFM analysis showed the average surface roughness of the NiO film as 2.21 nm. When $PbI_2$ was spun on top, the film roughness increased to 7.72 nm. This is caused by the formation of $PbI_2$ crystals (as evidenced in the SEM image) on top of NiO layer when the solvent, DMF, evaporated away. $PbI_2$ is a layered compound composed of I—Pb—I sheets; once dipped into $CH_3NH_3I$ isopropyl alcohol solution, $CH_3NH_3I$ immediately inserted into the sheet, forming the $CH_3NH_3PbI_3$ final product. This reaction is driven by the large formation energy of $CH_3NH_3PbI_3$ and accompanied by significant film thickness increase due to the growth of large $CH_3NH_3PbI_3$ grains. As shown in Figure 2c, the film remained crack- and pinhole-free; moreover, large crystals with dimensions of tens to 100 nanometers were abundantly scattered within the film. Transformation from $PbI_2$ to $CH_3NH_3PbI_3$ resulted in significant volume expansion, which diminished cracks and pinholes, as widely observed in the selenization of copper indium gallium disulfide nanoparticles into copper indium gallium diselenide films.[20] AFM measurement revealed an increased surface roughness of 21.2 nm. Such film morphology is similar to previous reports,[2,7] indicating a comparable quality of the $CH_3NH_3PbI_3$ film was obtained from this quick sequential deposition strategy.

X-ray diffraction measurements were carried out to study the transformation process, and the results are included in Figure 3a. Before treatment, hexagonal 2H prototype $PbI_2$ was obtained, as evidenced by the strong (001), (002), and (003) diffraction peaks. When the $PbI_2$ film was treated with $CH_3NH_3I$ for 5 s, very strong diffraction peaks indexed to tetragonal $CH_3NH_3PbI_3$ were observed, although there was some $PbI_2$ left unreacted. Prolonged treatment to 45 s reduced the $PbI_2$ diffraction peaks to very small intensities, suggesting the reaction between $PbI_2$ and $CH_3NH_3I$ was mostly finished.

A trace amount of leftover $PbI_2$ was also observed in the $CH_3NH_3PbI_3$ film produced through alternative approaches.[21] However, this material may not be very harmful because of its large band gap, just like the ZnS secondary phase in copper zinc tin sulfoselenide solar cells.[22] The grain size estimated from the Scherrer equation was approximately 75 nm, in good agreement with previous SEM observations. Previous study showed that quick conversion from $PbI_2$ to $CH_3NH_3PbI_3$ occurred only when $PbI_2$ was deposited into mesoporous $TiO_2$ scaffolding; when $PbI_2$ thin film was involved, this reaction took several hours to complete at room temperature.[7] In our case, this reaction took place at 70 °C. Elevated temperature substantially speeded up the insertion of $CH_3NH_3I$ into the $PbI_2$ layer, completing the transformation within 1 min.

Successful charge transfer from $CH_3NH_3PbI_3$ to NiO is a prerequisite to make efficient solar cells. We applied photoluminescence measurement to study this transferring process, and the result is shown in Figure 3b. When $CH_3NH_3PbI_3$ was deposited onto quartz glass, an inert substrate, strong photoluminescence from $CH_3NH_3PbI_3$ was observed centered at around 760 nm, similar to others' results.[7] However, when NiO was employed as the substrate, photoluminescence from $CH_3NH_3PbI_3$ deposited from an identical process was completely quenched. Clearly, free holes (or excitons) generated in $CH_3NH_3PbI_3$ upon illumination are extracted (or dissociated) by the underlying NiO layer, quenching the band edge photoluminescence. This observation indicates that NiO is indeed a good hole-collecting layer for perovskite solar cells.

Now we discuss our planar heterojunction photovoltaic device. The work function of the NiO layer depends heavily on the treatment history.[17,18] In our solution-processed NiO film, UV zone (UVO) treatment induced an obvious binding energy shift, from 16.19 to 15.94 eV (Figure 4a). This translated to a 0.25 eV work function deepening, from 5.03 eV before UVO treatment to 5.26 eV after UVO treatment. NiO is known to adsorb carbonaceous species and other atmospheric contaminants during storage, which could significantly reduce work function.[17] UVO treatment removed the surface adsorbents, exposed a clean NiO surface, and hence increased NiO work function. Our planar photovoltaic device architecture is ITO/NiO/$CH_3NH_3PbI_3$/PCBM/Al, and the corresponding band diagram and cross-sectional SEM images of the full device are shown in Figure 4b and c, respectively. NiO has an extremely deep valence band position at 6.5 eV and a shallow conduction band located at 2.1 eV relative to vacuum.[14] Obviously, NiO could act as an excellent hole-collecting layer and simultaneously block electrons. Upon illumination, electrons and holes are generated inside the $CH_3NH_3PbI_3$ absorber layer; electrons flow to PCBM and are collected by the Al electrode, and holes are selectively collected by NiO and move to ITO. In the SEM image, the $CH_3NH_3PbI_3$ layer was measured to be about 300 nm, and the planar NiO layer is hardly discernible because of its extremely small thickness. Ellipsometry measurement confirmed the NiO layer to be 10.2 nm using a 2% $Ni(CH_3COO)_2$ precursor solution.

Figure 5 presents device performance statistics of three batches of our devices and the current density−voltage (*J*−*V*) curves of the best devices. In order to study the effect of the NiO layer for hole collection in perovskite solar cells, three batches of devices using different materials including poly(3,4-ethylenedioxythiophene)−poly(styrenesulfonate) (PEDOT:PSS), a NiO layer without UVO treatment (NiO W/O UVO), and a NiO layer with UVO treatment (NiO with UVO) were measured and analyzed. For each type of devices, 18 cells were measured and the data were compiled. For PEDOT:PSS devices, shirt-circuit current density ($J_{sc}$) is 11.0 ± 1.4 mA/cm$^2$, open-circuit voltage ($V_{oc}$) is 0.75 ± 0.07 V, fill factor (FF) is 0.54 ± 0.03, and power conversion efficiency (PCE) is 4.5 ± 0.8% . For NiO W/O UVO devices, $J_{sc}$ is 11.8 ± 1.8 mA/cm$^2$, $V_{oc}$ is 0.84 ± 0.10 V, FF is 0.45 ± 0.05, and PCE is 4.4 ± 1.4%; for NiO with UVO devices, $J_{sc}$ is 13.1 ± 1.6 mA/cm$^2$, $V_{oc}$ is 0.95 ± 0.09 V, FF is 0.45 ± 0.05, and PCE is 5.9 ± 1.3%. As the control, the performance of our PEDOT:PSS device is comparable with the latest literature result[23] ($V_{oc}$ of 0.91 V, $J_{sc}$ of 10.8 mA/cm$^2$, FF of 0.76, and PCE of 7.4%). Clearly, devices employing a NiO layer all showed significantly higher $V_{oc}$, being 0.84 ± 0.10 and 0.95 ± 0.09 V for the NiO layer without and with UVO treatment, respectively, as compared to the 0.75 ± 0.07 V of the PEDOT:PSS device. PEDOT:PSS has a low work function of −5.0 eV, and the valence band maximum (VBM) of $CH_3NH_3PbI_3$ locates at −5.4 eV. Such an energy loss during charge transfer between $CH_3NH_3PbI_3$ and PEDOT:PSS accounted for the $V_{oc}$ deficiency. For NiO with

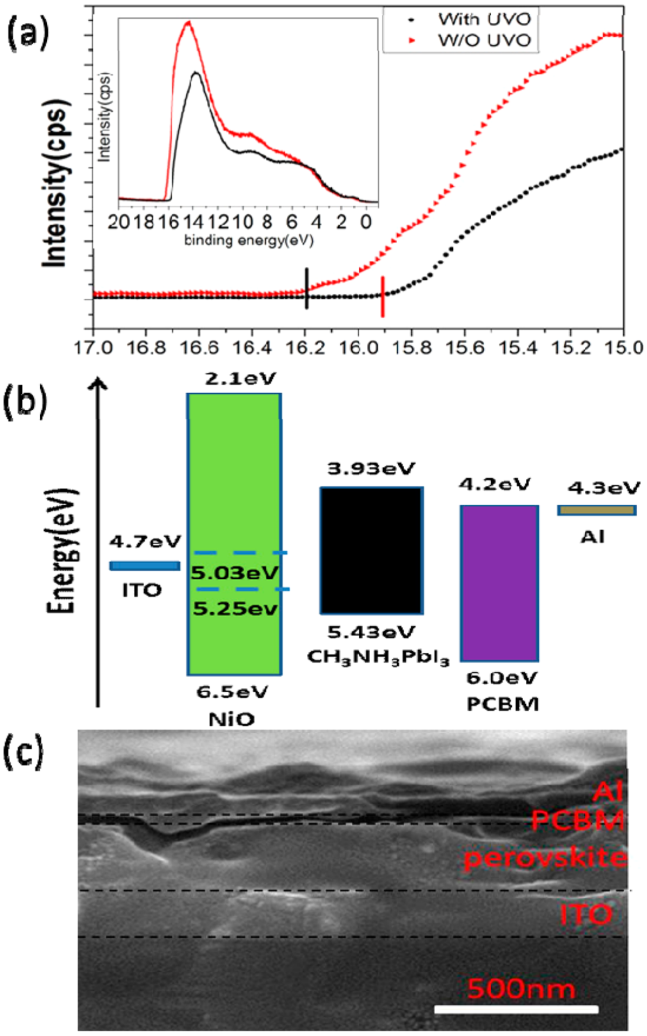

**Figure 4.** (a) Ultra photoelectron spectrum (UPS) results to determine NiO valence band position and work function. The inset is the full spectra. (b) Band diagram and (c) cross-sectional SEM image for our ITO/NiO/$CH_3NH_3PbI_3$/PCBM device. The NiO layer is invisible in panel c because of its extremely small thickness.

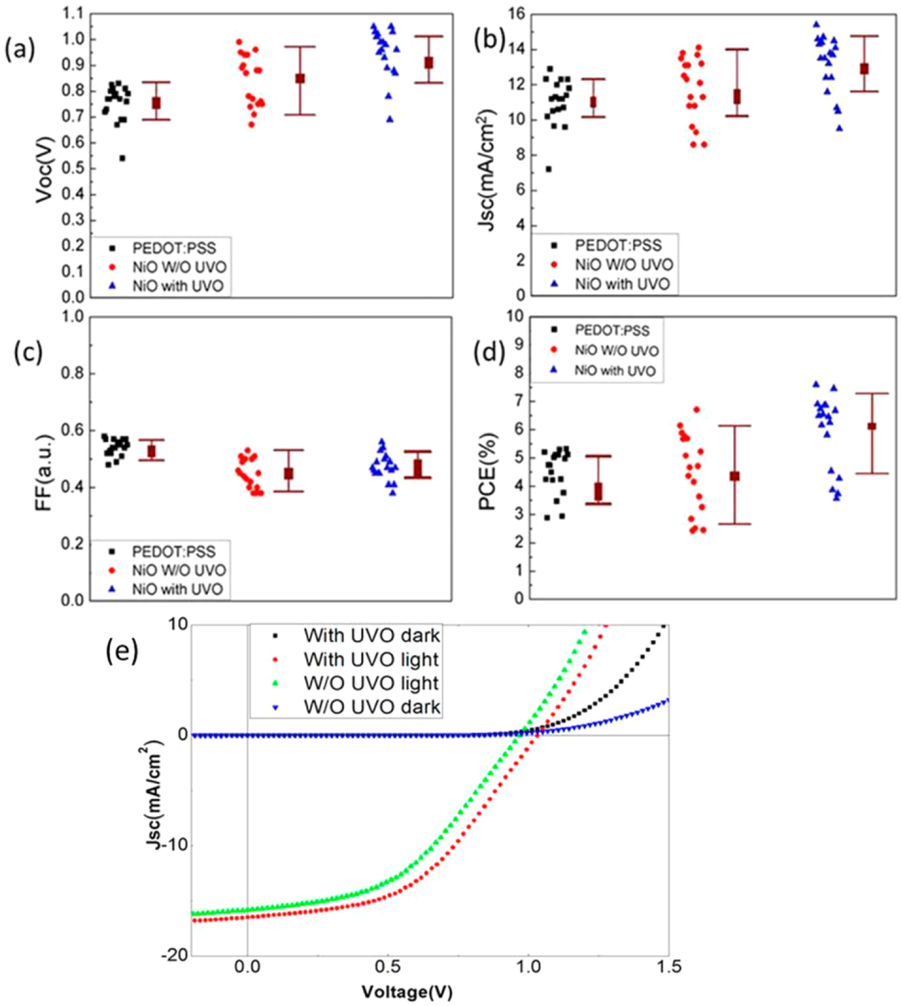

**Figure 5.** Statistics of device performance of 18 cells using PEDOT:PSS, a NiO layer without UVO treatment, and a NiO layer with UVO treatment as the hole-collecting layer: (a) $V_{oc}$, (b) $J_{sc}$, (c) FF. and (d) PCE. (e) $J$−$V$ curves of the best devices in the dark and under simulated 100 mW/cm$^2$ AM1.5G illumination.

**Table 1. Device Performance Using a UVO-Treated NiO Layer of Different Thicknesses**

| concentration (%) | thickness (nm) | $V_{oc}$ (V) | $J_{sc}$ (mA/cm$^2$) | FF | PCE (%) |
|---|---|---|---|---|---|
| 1 | 7.8 | 0.88 ± 0.18 | 11.9 ± 2.1 | 0.45 ± 0.04 | 5.2 ± 1.8 |
| 2 | 10.2 | 0.94 ± 0.10 | 13.1 ± 1.6 | 0.47 ± 0.04 | 5.9 ± 1.3 |
| 5 | 20.5 | 0.87 ± 0.20 | 11.9 ± 1.8 | 0.41 ± 0.05 | 4.8 ± 1.8 |
| 10 | 35.6 | 0.85 ± 0.18 | 11.2 ± 1.7 | 0.38 ± 0.06 | 3.9 ± 2.0 |
| 15 | 48.3 | 0.83 ± 0.17 | 6.3 ± 2.0 | 0.33 ± 0.07 | 3.3 ± 2.0 |

UVO treatment, the UPS measurement revealed that the Fermi energy and the VBM resided at −5.26 eV and −6.5 eV, respectively. Consequently, NiO-based photovoltaic devices showed higher $V_{oc}$ due to minimized energy loss. In addition, UVO treatment improved the $V_{oc}$ and $J_{sc}$ of solar cells as compared to the device employing NiO without UVO treatment, which was ascribed to the deepened work function of NiO and the better coverage of $CH_3NH_3PbI_3$ on the treated planar NiO layer.[24] Figure 5b shows the $J$−$V$ curves of the best device in the dark and under simulated 100 mW/cm$^2$ illumination. The best device has a $V_{oc}$ of 1.05 V, a $J_{sc}$ of 15.4 mA/cm$^2$, and a FF of 47%, corresponding to an efficiency of 7.6%.

We further studied the influence of NiO thickness on device performance. The thickness of the NiO layer was manipulated by tuning the weight percentage of $Ni(CH_3COO)_2$ in the precursor solution and measured by ellipsometry. Table 1 summarizes the device performance. Obviously, the 10.2 nm NiO devices showed the best $V_{oc}$, $J_{sc}$, and FF and hence the highest PCE. Devices employing a 7.8 nm thick NiO layer had slightly reduced device performance, while devices using a 48.3 nm thick NiO layer showed substantially deteriorated $J_{sc}$ and FF, leading to the worst PCE. A thick NiO film absorbs much incident light but contributes little to photocurrent, reducing $J_{sc}$; it also introduces large series resistance to the device due to its high resistivity nature, decreasing FF. A thin NiO film, on the other hand, probably has some voids with the underside of FTO exposed to $CH_3NH_3PbI_3$, which fails to selectively collect holes efficiently. As a result, a 2% $Ni(CH_3COO)_2$ solution produced the device with the best overall performance.

It should be noted that during the reviewing process of this paper, two similar papers using NiO as the hole collection and transportation layer were published by the Chen and Guo groups.[24,25] They first reported the deposition of $CH_3NH_3PbI_3$ onto a planar NiO layer through fast spin-coating (8000 rpm) and built a planar ITO/NiO/$CH_3NH_3PbI_3$/PCBM/BCP/Al (BCP stands for bathocuproine) device with 7.9% efficiency; they then incorporated a mesoporous NiO layer into the planar device and obtained a 9.51% device. They also found the UVO treatment was beneficial for their device, and the highest $V_{oc}$ they achieved was 1.04 V. These reports further echo our findings that NiO is indeed a very promising functional layer in perovskite solar cells.

In summary, we have built efficient perovskite solar cells using NiO as the hole-collecting layer. Employing a simple and quick sequential deposition strategy, we successfully fabricated a high-quality $CH_3NH_3PbI_3$ absorber onto a planar NiO film. Through film thickness optimization and UVO treatment, an inverted planar $CH_3NH_3PbI_3$ solar cell with a $V_{oc}$ of 1.05 V and efficiency of 7.6% was obtained. Compared with PEDOT:PSS, NiO has optimal band alignment with $CH_3NH_3PbI_3$, leading to a device with higher $V_{oc}$ and better efficiency. Our results showed the potential of NiO as the hole-collecting layer for organometal trihalide perovskite solar cells, and higher efficiency would be expected upon further optimization.

## ■ AUTHOR INFORMATION

### Corresponding Authors

*E-mail: wlma@suda.edu.cn.
*E-mail: jtang@mail.hust.edu.cn.

### Notes

The authors declare no competing financial interest.

## ■ ACKNOWLEDGMENTS

This work is financially supported by the seed project of Wuhan National Laboratory for Optoelectronics, by the "National 1000 Young Talents" project, by the National Natural Science Foundation of China (NSFC 61274055, 61322401), and the 973 Program of China (2011CBA00703). The Analytical and Testing Center of HUST and the Center for Nanoscale Characterization and Devices of WNLO are also acknowledged for the characterization support. We would also like to acknowledge Innovative Technology and Beijing Technol Science Co. Ltd. for glovebox and thermal evaporator technical assistance, respectively.

## ■ REFERENCES

(1) Kojima, A.; Teshima, K.; Shirai, Y.; Miyasaka, T. Organometal halide perovskites as visible-light sensitizers for photovoltaic cells. *J. Am. Chem. Soc.* **2009**, *131*, 6050−6051.

(2) Kim, H.-S.; Lee, C.-R.; Im, J.-H.; Lee, K.-B.; Moehl, T.; Marchioro, A.; Moon, S.-J.; Humphry-Baker, R.; Yum, J.-H.; Moser, J. E.; Graetzel, M.; Park, N.-G. Lead iodide perovskite sensitized all-solid-state submicron thin film mesoscopic solar cell with efficiency exceeding 9%. *Sci. Rep.* **2012**, *2*, 592.

(3) Cai, B.; Xing, Y.; Yang, Z.; Zhang, W.-H.; Qiu, J. High performance hybrid solar cells sensitized by organolead halide perovskites. *Energy Environ. Sci.* **2013**, *6*, 1480−1485.

(4) Noh, J. H.; Im, S. H.; Heo, J. H.; Mandal, T. N.; Seok, S. I. Chemical management for colorful, efficient, and stable inorganic-organic hybrid nanostructured solar cells. *Nano Lett.* **2013**, *13*, 1764−1769.

(5) Liu, M.; Johnston, M. B.; Snaith, H. J. Efficient planar heterojunction perovskite solar cells by vapour deposition. *Nature* **2013**, *501*, 395−398.

(6) Liu, D.; Kelly, T. L. Perovskite solar cells with a planar heterojunction structure prepared using room-temperature solution processing techniques. *Nat. Photonics* **2014**, *8*, 133−138.

(7) Burschka, J.; Pellet, N.; Moon, S.-J.; Humphry-Baker, R.; Gao, P.; Nazeeruddin, M. K.; Gratzel, M. Sequential deposition as a route to high-performance perovskite-sensitized solar cells. *Nature* **2013**, *499*, 316−319.

(8) Snaith, H. J. Perovskites: the emergence of a new era for low-cost, high-efficiency solar cells. *J. Phys. Chem. Lett.* **2013**, *4*, 3623−3630.

(9) Hodes, G. Perovskite-based solar cells. *Science* **2013**, *342*, 317−318.

(10) Xing, G.; Mathews, N.; Sun, S.; Lim, S. S.; Lam, Y. M.; Grätzel, M.; Mhaisalkar, S.; Sum, T. C. Long-range balanced electron- and hole-transport lengths in organic-inorganic $CH_3NH_3PbI_3$. *Science* **2013**, *342*, 344−347.

(11) Stranks, S. D.; Eperon, G. E.; Grancini, G.; Menelaou, C.; Alcocer, M. J. P.; Leijtens, T.; Herz, L. M.; Petrozza, A.; Snaith, H. J. Electron-hole diffusion lengths exceeding 1 micrometer in an organometal trihalide perovskite absorber. *Science* **2013**, *342*, 341−344.

(12) Jeng, J. Y.; Chiang, Y. F.; Lee, M. H.; Peng, S. R.; Guo, T. F.; Chen, P.; Wen, T. C. $CH_3NH_3PbI_3$ perovskite/fullerene planar-heterojunction hybrid solar cells. *Adv. Mater.* **2013**, *25*, 3727−3732.

(13) Docampo, P.; Ball, J. M.; Darwich, M.; Eperon, G. E.; Snaith, H. J. Efficient organometal trihalide perovskite planar-heterojunction solar cells on flexible polymer substrates. *Nat. Commun.* **2013**, *4*, 2761.

(14) Irwin, M. D.; Buchholz, B.; Hains, A. W.; Chang, R. P. H.; Marks, T. J. p-Type semiconducting nickel oxide as an efficiency-enhancing anode interfacial layer in polymer bulk-heterojunction solar cells. *Proc. Natl. Acad. Sci. U.S.A.* **2008**, *105*, 2783−2787.

(15) Steirer, K. X.; Chesin, J. P.; Widjonarko, N. E.; Berry, J. J.; Miedaner, A.; Ginley, D. S.; Olson, D. C. Solution deposited NiO thin-films as hole transport layers in organic photovoltaics. *Org. Electron.* **2010**, *11*, 1414−1418.

(16) Leijtens, T.; Eperon, G. E.; Pathak, S.; Abate, A.; Lee, M. M.; Snaith, H. J. Overcoming ultraviolet light instability of sensitized $TiO_2$ with meso-superstructured organometal tri-halide perovskite solar cells. *Nat. Commun.* **2013**, *4*, 2885.

(17) Greiner, M. T.; Helander, M. G.; Wang, Z.-B.; Tang, W.-M.; Lu, Z.-H. Effects of processing conditions on the work function and energy-level alignment of NiO thin films. *J. Phys.Chem. C* **2010**, *114*, 19777−19781.

(18) Zhai, Z.; Huang, X.; Xu, M.; Yuan, J.; Peng, J.; Ma, W. Greatly reduced processing temperature for a solution-processed NiOx buffer layer in polymer solar cells. *Adv. Energy Mater.* **2013**, *3*, 1614−1622.

(19) Uehara, S.; Sumikura, S.; Suzuki, E.; Mori, S. Retardation of electron injection at NiO/dye/electrolyte interface by aluminium alkoxide treatment. *Energy Environ. Sci.* **2010**, *3*, 641−644.

(20) Guo, Q.; Ford, G. M.; Hillhouse, H. W.; Agrawal, R. Sulfide nanocrystal inks for dense $Cu(In_{1-x}Ga_x)(S_{1-y}Se_y)_2$ absorber films and their photovoltaic performance. *Nano Lett.* **2009**, *9*, 3060−3065.

(21) Chen, Q.; Zhou, H.; Hong, Z.; Luo, S.; Duan, H.-S.; Wang, H.-H.; Liu, Y.; Li, G.; Yang, Y. Planar heterojunction perovskite solar cells via vapor-assisted solution process. *J. Am. Chem. Soc.* **2014**, *16*, 622−625.

(22) Todorov, T. K.; Tang, J.; Bag, S.; Gunawan, O.; Gokmen, T.; Zhu, Y.; Mitzi, D. B. Beyond 11% efficiency: characteristics of state-of-the-art $Cu_2ZnSn(S,Se)_4$ solar cells. *Adv. Energy Mater.* **2013**, *3*, 34−338.

(23) Sun, S.; Salim, T.; Mathews, N.; Duchamp, M.; Boothroyd, C.; Xing, G.; Sum, T. C.; Lam, Y. M. The origin of high efficiency in low-temperature solution-processable bilayer organometal halide hybrid solar cells. *Energy Environ. Sci.* **2014**, *7*, 399−407.

(24) Jeng, J. Y.; Chiang, Y. F.; Lee, M. H.; Peng, S. R.; Guo, T. F.; Chen, P.; Wen, T. C. $CH_3NH_3PbI_3$ perovskite/fullerene planar-heterojunction hybrid solar cells. *Adv. Mater.* **2013**, *25*, 3727−3732.

(25) Wang, K. C.; Jeng, J. Y.; Shen, P. S.; Chang, Y. C.; Diau, E. W.; Tsai, C. H.; Chao, T. Y.; Hsu, H. C.; Lin, P. Y.; Chen, P.; Guo, T. F.; Wen, T. C. p-Type mesoscopic nickel oxide/organometallic perovskite heterojunction solar cells. *Sci. Rep.* **2014**, *4*, 4756.